

9. N. Zenkin, Y. Yuzenkova, K. Severinov, *Science* **313**, 518 (2006).
10. C. D. Kuhn *et al.*, *Cell* **131**, 1260 (2007).
11. D. Wang *et al.*, *Science* **324**, 1203 (2009).
12. Materials and methods are available as supplementary materials on *Science* Online.
13. N. Zenkin, T. Naryshkina, K. Kuznedelov, K. Severinov, *Nature* **439**, 617 (2006).
14. S. K. Whitehall, C. Bardeleben, G. A. Kassavetis, *J. Biol. Chem.* **269**, 2299 (1994).
15. T. D. Yager, P. H. von Hippel, *Biochemistry* **30**, 1097 (1991).
16. W. S. Yarnell, J. W. Roberts, *Science* **284**, 611 (1999).
17. N. Komissarova, J. Becker, S. Solter, M. Kireeva, M. Kashlev, *Mol. Cell* **10**, 1151 (2002).
18. E. Zaychikov *et al.*, *Science* **273**, 107 (1996).
19. K. D. Westover, D. A. Bushnell, R. D. Kornberg, *Cell* **119**, 481 (2004).
20. T. J. Santangelo, J. W. Roberts, *Mol. Cell* **14**, 117 (2004).
21. M. H. Larson, W. J. Greenleaf, R. Landick, S. M. Block, *Cell* **132**, 971 (2008).
22. V. Epshtein, C. J. Cardinale, A. E. Ruckenstein, S. Borukhov, E. Nudler, *Mol. Cell* **28**, 991 (2007).

**Acknowledgments:** This work is dedicated to the memory of Denis Izyumov. We thank J. Roberts, E. Nudler, P. E. Geiduschek, and J. Brown for critical reading of the paper; G. Kassavetis, R. van Nues, H. Murray, N. Proudfoot, and P. Braglia for experimental advice; and J. Chong for help with *Archaea*. This work was supported by the UK

Biotechnology and Biological Sciences Research Council, the Biotechnology and Biological Sciences Research Council under the SysMO initiative, and the European Research Council [grant ERC-2007-StG 202994-MTP]. Data are available in the supplementary materials.

### Supplementary Materials

www.sciencemag.org/cgi/content/full/340/6140/1577/DC1  
Materials and Methods  
Supplementary Text  
Figs. S1 to S8  
Table S1  
References (23–27)

18 March 2013; accepted 13 May 2013  
10.1126/science.1237934

# Transcription Under Torsion

Jie Ma,<sup>1,2</sup> Lu Bai,<sup>3,4</sup> Michelle D. Wang<sup>1,2\*</sup>

In cells, RNA polymerase (RNAP) must transcribe supercoiled DNA, whose torsional state is constantly changing, but how RNAP deals with DNA supercoiling remains elusive. We report direct measurements of individual *Escherichia coli* RNAPs as they transcribed supercoiled DNA. We found that a resisting torque slowed RNAP and increased its pause frequency and duration. RNAP was able to generate  $11 \pm 4$  piconewton-nanometers (mean  $\pm$  standard deviation) of torque before stalling, an amount sufficient to melt DNA of arbitrary sequence and establish RNAP as a more potent torsional motor than previously known. A stalled RNAP was able to resume transcription upon torque relaxation, and transcribing RNAP was resilient to transient torque fluctuations. These results provide a quantitative framework for understanding how dynamic modification of DNA supercoiling regulates transcription.

DNA supercoiling is a regulator of gene expression (1–5). RNA polymerase (RNAP) must transcribe supercoiled DNA, and transcription elongation, in turn, generates DNA supercoiling. As RNAP moves along the helical groove of DNA, it generates (+) DNA supercoiling ahead and (–) DNA supercoiling behind (the “twin supercoiled domain model”) (1, 3–6). DNA supercoiling is broadly present during transcription (3–5). Active transcription can accumulate dynamic DNA supercoiling on DNA templates that are not bound by topological constraints (3), as well as in the presence of a normal complement of topoisomerases *in vivo* (4). However, little is known about some basic properties of the interplay between transcription and DNA supercoiling. We have developed an assay to directly monitor RNAP translocation in real time as it worked under a defined torque. An RNAP was torsionally anchored to the surface of a coverslip, and either the downstream or upstream end of the DNA template was torsionally anchored to the bottom of a nanofabricated quartz cylinder held in an angular optical trap (AOT) (Fig. 1A and fig. S1) (7–11). An AOT allows simultaneous control and measurement of rotation, torque, displacement, and force of the trapped cylinder (8–11). Analysis of these mea-

surements allowed for the determination of the RNAP position on the DNA template as it transcribed under torque (11).

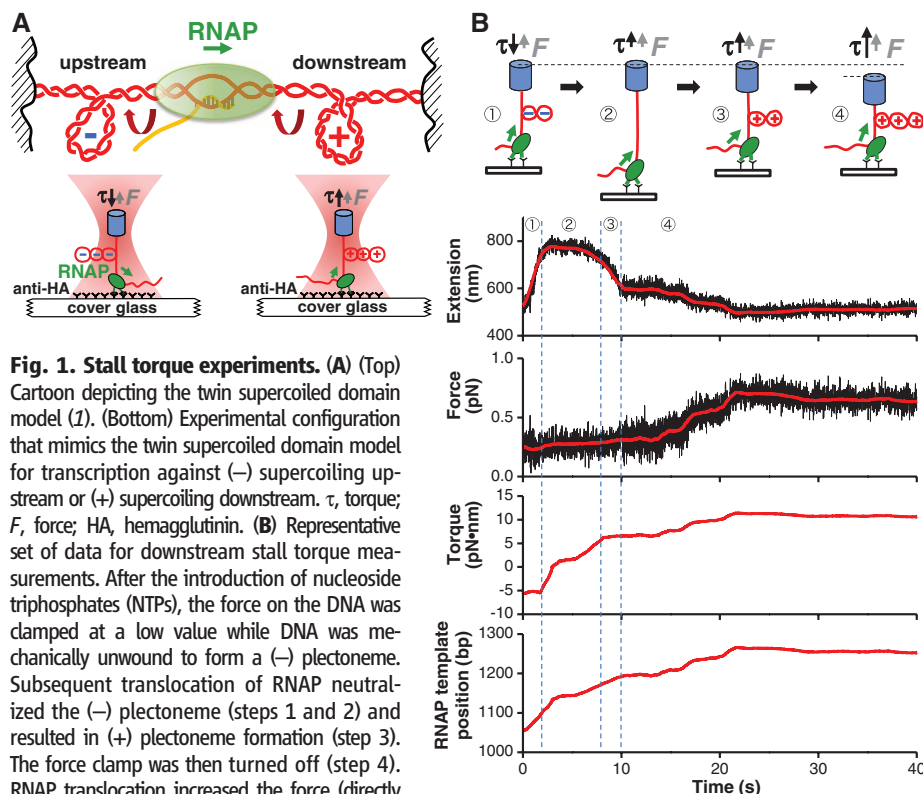


**Fig. 1. Stall torque experiments.** (A) (Top) Cartoon depicting the twin supercoiled domain model (1). (Bottom) Experimental configuration that mimics the twin supercoiled domain model for transcription against (–) supercoiling upstream or (+) supercoiling downstream.  $\tau$ , torque;  $F$ , force; HA, hemagglutinin. (B) Representative set of data for downstream stall torque measurements. After the introduction of nucleoside triphosphates (NTPs), the force on the DNA was clamped at a low value while DNA was mechanically unwound to form a (–) plectoneme. Subsequent translocation of RNAP neutralized the (–) plectoneme (steps 1 and 2) and resulted in (+) plectoneme formation (step 3). The force clamp was then turned off (step 4). RNAP translocation increased the force (directly measured) and the corresponding torque (derived) (11) until reaching a stall [ $<1$  base pair (bp)/s for 20 to 50 s]. Data were filtered: extension to 200 Hz (black) and 1 Hz (red) and force to 40 Hz (black) and 1 Hz (red). The RNAP template position is defined as the distance of RNAP from the transcription start site (in base pairs).

<sup>1</sup>Department of Physics–Laboratory of Atomic and Solid State Physics, Cornell University, Ithaca, NY 14853, USA. <sup>2</sup>Howard Hughes Medical Institute, Cornell University, Ithaca, NY 14853, USA. <sup>3</sup>Department of Biochemistry and Molecular Biology, Pennsylvania State University, University Park, PA 16801, USA. <sup>4</sup>Department of Physics, Pennsylvania State University, University Park, PA 16801, USA.

\*Corresponding author. E-mail: mwang@physics.cornell.edu

The measured downstream stall torque distribution is well fit by a Gaussian function, yielding a mean torque of  $11.0 \pm 3.7$  pN·nm (mean  $\pm$  SD), with the largest measured value being  $\sim 18$  pN·nm (Fig. 2A and fig. S6A). This mean torque is sufficient to create (+) plectonemic DNA under the low forces used in our experiments. In contrast, the upstream stall torque distribution shows an

asymmetry (Fig. 2B and fig. S6B). Unlike (+) supercoiled DNA, which can sustain a much higher torque before structural changes, (-) supercoiled DNA undergoes a transition at 10.5 pN·nm consistent with melting (fig. S3) (11). The upstream stall torque distribution shows a singular peak immediately before a sharp cutoff near the DNA melting torque, and  $\sim 60\%$  of RNAPs were stalled

between 10 to 12 pN·nm. These data indicate that RNAP is able to generate an upstream torque sufficient to alter DNA structure. The upstream data were fit with a Gaussian function, yielding a Gaussian centered at  $10.6 \pm 4.1$  pN·nm, comparable to the downstream stall torque (Fig. 2B). The spreads in the measured stall torque distributions are attributed to DNA sequence

### Fig. 2. Transcription stalling and resumption.

(A) Distribution of the measured downstream stall torques. The smooth blue curve is a fit with a Gaussian function, yielding a mean of  $11.0 \pm 3.7$  pN·nm (mean  $\pm$  SD). (B) Distribution of measured upstream stall torques. The smooth curve is a fit with a Gaussian function assuming that the peaked fraction generated torques of at least 10 pN·nm, yielding a mean of  $10.6 \pm 4.1$  pN·nm (mean  $\pm$  SD). (C) Example traces showing RNAP reverse translocation upon stalling. Both axes are shifted for clarity. For each trace, the arrow indicates the entry into a stall. (D) Fraction of RNAPs that resumed transcription after torque release versus time. After stalling, torque on RNAP was relaxed, and transcription was detected by an experiment similar to that shown in step 1 of Fig. 1B. Error bars indicate SEM.

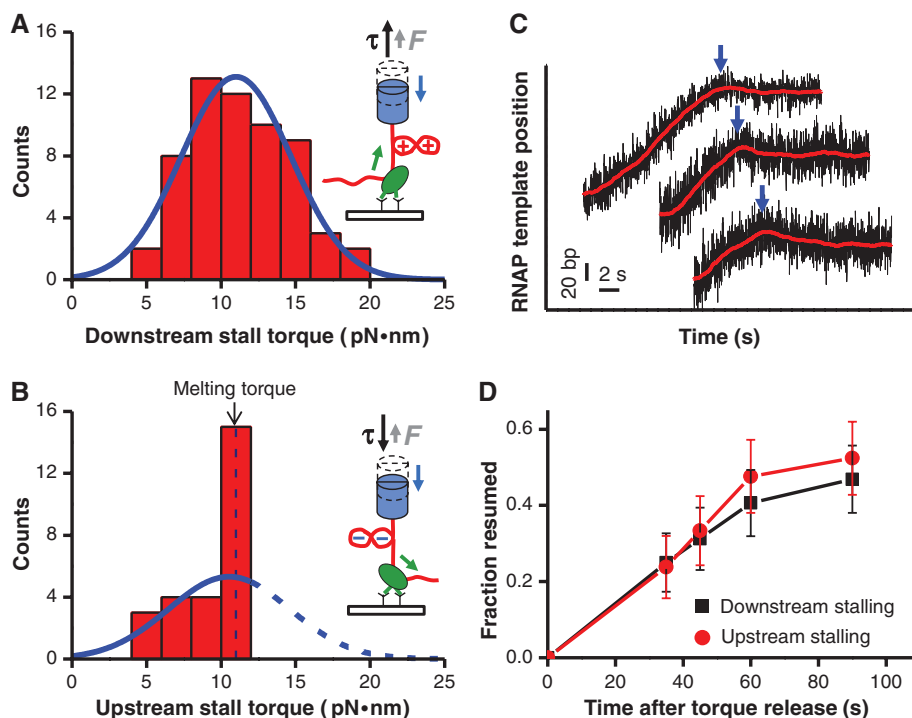
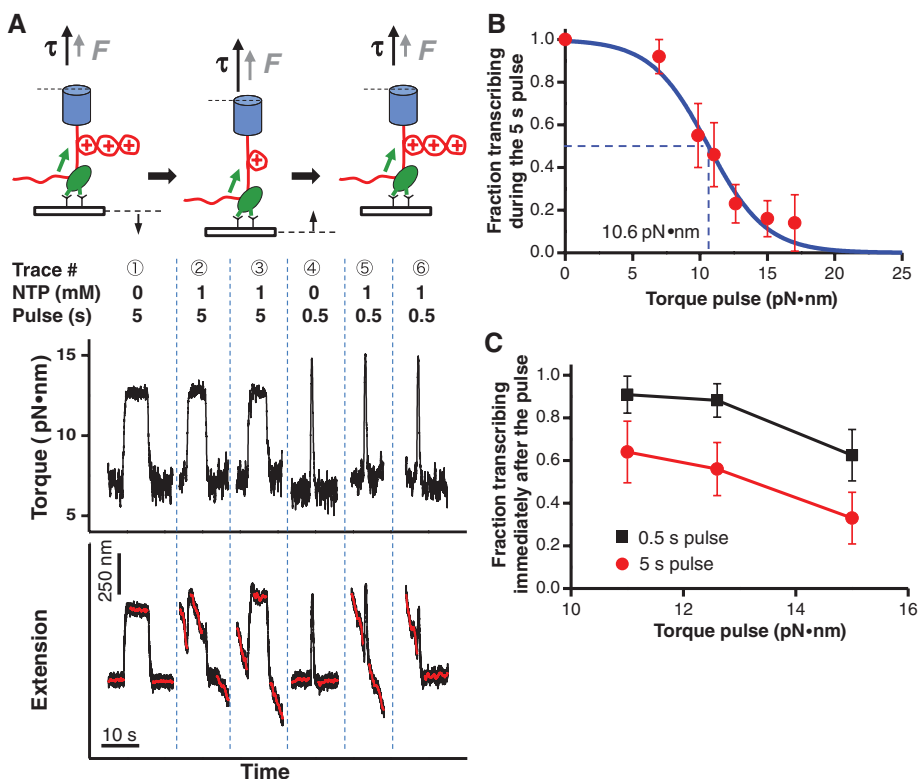


### Fig. 3. Transcription response to a transient torque pulse.

(A) (Top) Cartoon illustrating steps of the torque pulse experiments and (bottom) representative traces of data. RNAP initially transcribed under a low downstream torque of  $\sim 7$  pN·nm and then was subjected to a higher torque pulse for either 5 or 0.5 s before restoration of the initial low torque. Traces 1 and 4 are controls. The extension and time axes are shifted for clarity. (B) Probability of maintaining active transcription during the 5-s torque pulse. The blue solid line is a fit to a Boltzmann function:  $f = 1/[1 + e^{(\tau - \tau_c)/\tau_0}]$ , where  $\tau_c$  is the characteristic cutoff torque, and  $\tau_0$  is the characteristic width of the transition torque. Error bars indicate SEM. (C) Probability of resuming transcription immediately (within 5 s) after the torque pulse. Error bars indicate SEM.



variations and single-molecule stochasticity, according to a thermal-ratchet kinetic model for transcription elongation that we previously developed (15–17).

Thus, RNAP is fully capable of generating torque sufficient to melt DNA of arbitrary sequence (11), not just AT-rich sequences that are prone to melting (3, 4, 11). The strong (–) supercoiling generated by RNAP may facilitate initiation of transcription from adjacent promoters (18), binding of regulatory proteins (3, 4), and initiation of replication (19).

We found that, in some traces, RNAP reverse translocated upon stalling (Fig. 2C). This reverse

motion suggests that torque may induce stalling via backtracking, during which RNAP translocates back along the template DNA and displaces the 3' transcript from the active site, preventing RNA synthesis (20–22).

In vivo, torsional stress accumulated by RNAP may be relaxed by the arrival of a topoisomerase at the DNA template or by DNA rotation. We found that stalled RNAPs gradually resumed transcription following torque release (Fig. 2D). At 90 s after torque release, ~50% of stalled RNAPs had resumed transcription. Thus, in vivo torque relaxation should allow a large fraction of stalled RNAPs to resume transcription, prevent-

ing them from becoming obstacles or inducing DNA damage that disrupts genome stability (23).

In vivo, torsional stress in local DNA segments may be present transiently due to actions of motor proteins and dynamic reconfiguration of topological domains. However, it is not known how these sudden changes in torsional stress might influence a transcribing RNAP. We thus carried out transient torque pulse experiments to determine how RNAP responded to a brief exposure of a resisting torque on a time scale comparable to those of topoisomerases (24–26) (0.5 or 5 s) (Fig. 3A). We found that the fraction of active RNAPs during the 5-s pulse decreased as the torque was jumped to an increasingly higher value (Fig. 3B). The characteristic cutoff torque was  $10.6 \pm 4.0$  pN·nm, a value similar to the mean stall torque. A substantially larger fraction of RNAPs was able to transcribe immediately (within 5 s) after the 0.5-s pulse, as opposed to after the 5-s pulse (Fig. 3C), indicating that a 0.5-s torque pulse does not give sufficient time for RNAP to backtrack substantially. Thus, RNAP can effectively resist transient torque fluctuations (<0.5 s) but is unable to withstand prolonged exposure to a large torque without stalling or arresting.

We investigated the torque-velocity relationship, which characterizes how the transcription speed is regulated by torque (Fig. 4A). To maintain a constant torque, we monitored transcription in the presence of a DNA plectoneme under a small and constant force. The measured transcription traces showed that continuous elongation was interrupted by frequent pausing (Fig. 4B and fig. S7). Because of the sensitivity of the assay, it was possible to resolve pauses as short as 0.2 s. By analyzing the velocity between pauses, we obtained the torque-velocity relation of RNAP. Figure 4C shows how the transcription rate increased with an assisting torque and decreased with a resisting torque. In addition, both pause density and duration decreased with an assisting torque and increased with a resisting torque (Fig. 4D).

We show that RNAP can generate torque; torque, in turn, regulates transcription rate and pausing; and excessive torque accumulation leads to transcription stalling and DNA structural alteration. A transcription-generated supercoiling wave can propagate through DNA to provide action at a distance, not only to alter DNA structure (3, 4) but also to potentially alter or dissociate bound proteins (3, 4, 27). Torsion generated by eukaryotic RNAP may alter chromatin fiber and evict histones (4, 27, 28), and torsional relaxation by chromatin may, in turn, facilitate transcription (28).

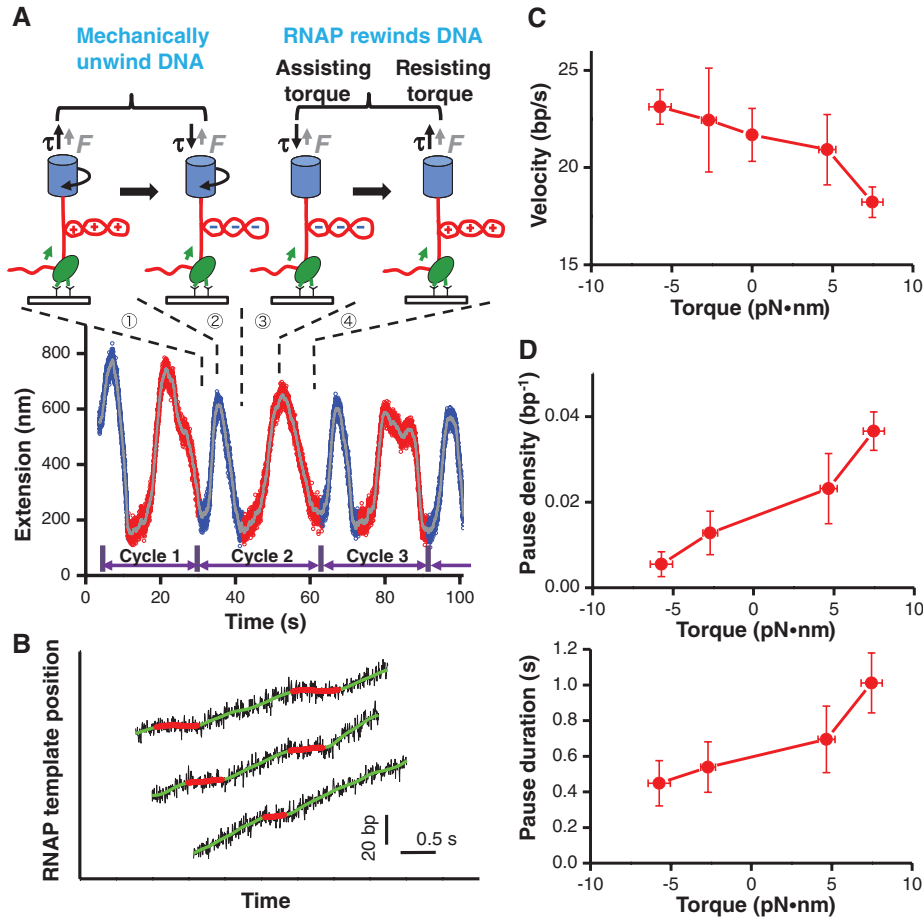


**Fig. 4. Determination of transcription torque-velocity relationship.** (A) Representative set of data for transcription measurement under a constant torque. Transcribing RNAP, under a small and constant tension of 0.15 pN, was subjected to multiple cycles of resisting and assisting torque. For each cycle, the downstream DNA was mechanically unwound to remove any (+) plectoneme (step 1) and create a (–) plectoneme (step 2). Subsequent RNAP transcription was assisted by the (–) DNA supercoiling (step 3), until the generation of (+) supercoiling, which hindered transcription (step 4). In the presence of a plectoneme, the torque on the DNA was constant for a given force (9) (fig. S3), and RNAP velocity was derived from the slope of the extension-versus-time curve (11). Also, we define a resisting torque to be (+) and an assisting torque to be (–). Data were filtered to 200 Hz (blue and red) and 1 Hz (gray). (B) Representative transcription traces under a torque of +7.5 pN·nm. Continuous transcription (green smoothed data) was interrupted by pauses (red smoothed data). (C) Transcription torque-velocity relationship. Transcription velocity was obtained by weighting each transcript position equally, and the resulting velocity reflected primarily transcription rates between pauses (11, 29). Vertical error bars indicate SEM; horizontal error bars denote SD. (D) Pause density (top) and duration (bottom) as a function of torque. A pause is defined as having a duration of  $\geq 0.2$  s at a given nucleotide position (11). Zero-torque data (fig. S8) had lower sensitivity to transcription due to lack of plectonemes in DNA, precluding detection of pauses of 0.2 to 2 s in duration, and were thus excluded from pause analysis. Vertical error bars indicate SEM; horizontal error bars denote SD.

References and Notes

1. L. F. Liu, J. C. Wang, *Proc. Natl. Acad. Sci. U.S.A.* **84**, 7024 (1987).
2. A. Travers, G. Muskhelishvili, *Nat. Rev. Microbiol.* **3**, 157 (2005).
3. F. Kouzine, J. Liu, S. Sanford, H.-J. Chung, D. Levens, *Nat. Struct. Mol. Biol.* **11**, 1092 (2004).
4. F. Kouzine, S. Sanford, Z. Elisha-Feil, D. Levens, *Nat. Struct. Mol. Biol.* **15**, 146 (2008).

5. K. Matsumoto, S. Hirose, *J. Cell Sci.* **117**, 3797 (2004).
6. H.-Y. Wu, S. H. Shyy, J. C. Wang, L. F. Liu, *Cell* **53**, 433 (1988).
7. A. La Porta, M. D. Wang, *Phys. Rev. Lett.* **92**, 190801 (2004).
8. C. Deufel, S. Forth, C. R. Simmons, S. Dejosha, M. D. Wang, *Nat. Methods* **4**, 223 (2007).
9. S. Forth *et al.*, *Phys. Rev. Lett.* **100**, 148301 (2008).
10. M. Y. Sheinin, S. Forth, J. F. Marko, M. D. Wang, *Phys. Rev. Lett.* **107**, 108102 (2011).
11. Materials and methods are available as supplementary materials on Science Online.
12. Y. Harada *et al.*, *Nature* **409**, 113 (2001).
13. A. Revyakin, R. H. Ebricht, T. R. Strick, *Proc. Natl. Acad. Sci. U.S.A.* **101**, 4776 (2004).
14. A. Revyakin, C. Liu, R. H. Ebricht, T. R. Strick, *Science* **314**, 1139 (2006).
15. L. Bai, A. Shundrovsky, M. D. Wang, *J. Mol. Biol.* **344**, 335 (2004).
16. L. Bai, R. M. Fulbright, M. D. Wang, *Phys. Rev. Lett.* **98**, 068103 (2007).
17. L. Bai, M. D. Wang, *J. Stat. Mech.* **2010**, P12007 (2010).
18. D. M. J. Lilley, C. F. Higgins, *Mol. Microbiol.* **5**, 779 (1991).
19. D. Kowalski, M. J. Eddy, *EMBO J.* **8**, 4335 (1989).
20. N. Komissarova, M. Kashlev, *Proc. Natl. Acad. Sci. U.S.A.* **94**, 1755 (1997).
21. J. W. Shaevitz, E. A. Abbondanzieri, R. Landick, S. M. Block, *Nature* **426**, 684 (2003).
22. E. A. Galbur *et al.*, *Nature* **446**, 820 (2007).
23. D. Dutta, K. Shatalin, V. Epshtein, M. E. Gottesman, E. Nudler, *Cell* **146**, 533 (2011).
24. T. R. Strick, V. Croquette, D. Bensimon, *Nature* **404**, 901 (2000).
25. D. A. Koster, V. Croquette, C. Dekker, S. Shuman, N. H. Dekker, *Nature* **434**, 671 (2005).
26. J. Gore *et al.*, *Nature* **439**, 100 (2006).
27. V. Levchenko, B. Jackson, V. Jackson, *Biochemistry* **44**, 5357 (2005).
28. C. Lavelle, *Biochimie* **89**, 516 (2007).
29. K. Adelman *et al.*, *Proc. Natl. Acad. Sci. U.S.A.* **99**, 13538 (2002).

**Acknowledgments:** We thank members of the Wang lab for critical reading of the manuscript. We especially thank R. M. Fulbright for purification of the RNAP and S. Forth, Y. Yang, M. Y. Sheinin, J. T. Inman, and R. A. Forties for assistance with single-molecule assays, data acquisition, data analysis, and figure preparation. We wish to acknowledge support from an NIH grant (GM059849 to M.D.W) and an NSF grant (MCB-0820293 to M.D.W).

#### Supplementary Materials

www.sciencemag.org/cgi/content/full/340/6140/1580/DC1  
Materials and Methods  
Figs. S1 to S11  
References (30–51)  
Movie S1

21 January 2013; accepted 21 May 2013  
10.1126/science.1235441

## Fe-S Cluster Biosynthesis Controls Uptake of Aminoglycosides in a ROS-Less Death Pathway

Benjamin Ezraty,<sup>1</sup> Alexandra Vergnes,<sup>1</sup> Manuel Banzhaf,<sup>2</sup> Yohann Duverger,<sup>1</sup> Allison Huguenot,<sup>1</sup> Ana Rita Brochado,<sup>2</sup> Shu-Yi Su,<sup>2</sup> Leon Espinosa,<sup>1</sup> Laurent Loiseau,<sup>1</sup> Béatrice Py,<sup>1</sup> Athanasios Typas,<sup>2</sup> Frédéric Barras<sup>1\*</sup>

All bactericidal antibiotics were recently proposed to kill by inducing reactive oxygen species (ROS) production, causing destabilization of iron-sulfur (Fe-S) clusters and generating Fenton chemistry. We find that the ROS response is dispensable upon treatment with bactericidal antibiotics. Furthermore, we demonstrate that Fe-S clusters are required for killing only by aminoglycosides. In contrast to cells, using the major Fe-S cluster biosynthesis machinery, ISC, cells using the alternative machinery, SUF, cannot efficiently mature respiratory complexes I and II, resulting in impendence of the proton motive force (PMF), which is required for bactericidal aminoglycoside uptake. Similarly, during iron limitation, cells become intrinsically resistant to aminoglycosides by switching from ISC to SUF and down-regulating both respiratory complexes. We conclude that Fe-S proteins promote aminoglycoside killing by enabling their uptake.

Reactive oxygen species (ROS) have been recently proposed to be central to cell killing by all classes of bactericidal antibiotics (1). However, using a recently published high-throughput chemical-genetics screen in *Escherichia coli*, we did not detect any functional enrichment for ROS-defense genes in the profiles of two major classes of bactericidal antibiotics:  $\beta$ -lactams, which target the cell wall, and aminoglycosides, which cause mistranslation (fig. S1) (2). Instead,  $\beta$ -lactams and aminoglycosides cause cellular death through unrelated morphological defects (3–5) (fig. S2). We decided to further explore the proposed role of ROS in antibiotic killing by using a series of mutants altered in the protective response of *E. coli* against ROS and testing them with a  $\beta$ -lactam [ampicillin (Amp)] and an aminoglycoside [gentamicin (Gm)] antibiotic.

*E. coli* mutants, hypersensitive to  $O_2^-$  (lacking both cytoplasmic superoxide dismutases,  $\Delta sodA$  and  $\Delta sodB$ ) or to  $H_2O_2$  (lacking the  $H_2O_2$ -sensing master activator,  $\Delta oxyR$ ), exhibited similar sensitivities to Gm and Amp as the wild type (WT) in a time-dependent killing experiment, with  $\Delta oxyR$  being more resistant to Amp at the last time point, 4.5 hours after drug addition (Fig. 1, A and B). When tested in a concentration-dependent killing experiment, the two mutants were as sensitive as WT to Gm (Fig. 1C) but exhibited small differences to the WT at intermediate Amp concentrations, at levels that provided no support for a prominent role for ROS defense mechanisms during treatment with bactericidal antibiotics (Fig. 1D). In contrast and as expected, both strains were hypersensitive to their respective ROS source, a known  $O_2^-$  generator (paraquat) and  $H_2O_2$  (fig. S3). Similarly, an *oxyRc* strain constitutively expressing the OxyR regulon—which is significantly more resistant to  $H_2O_2$  (fig. S3)—showed slight differences to WT in killing experiments with Amp and Gm (Fig. 1, A to D), tending to be more susceptible to both antibiotics than WT (Fig. 1, C and D).

The lack of evidence for a link between oxidative stress and bactericidal antibiotics also held true when testing the same strains for minimal inhibitory concentrations (MIC) and growth rates in subinhibitory antibiotic amounts (table S1 and fig. S4). Taken together, these results revealed no association between ROS and bactericidal antibiotic sensitivity, in agreement with two recent reports using complementary approaches (6, 7).

Kohanski *et al.* (1) proposed that protein-bound Fe-S clusters are required for killing by bactericidal antibiotics because they release  $Fe^{2+}$  ions that fuel ROS production by Fenton chemistry. This assumption was based on the fact that mutants lacking the major Fe-S cluster biogenesis system ISC were resistant to both Gm and Amp. The *iscS* gene codes for the ISC cysteine desulfurase that, in addition to Fe-S protein maturation, is involved in all sulfur trafficking pathways (8, 9). We found that the *iscS* mutant, as previously reported (1), was fully resistant to Gm killing and showed partial resistance to Amp in a time-dependent killing experiment using 5  $\mu$ g/ml for both drugs (Fig. 2, A and B). However, the enhanced resistance of the *iscS* mutant was only recapitulated for Gm, but not for Amp at lower antibiotic concentrations (fig. S5, A and B) or when measuring MICs and growth rates in subinhibitory antibiotic concentrations (table S1 and fig. S5C).

We then tested an *iscUA* mutant, because in contrast to the pleiotropic *iscS* mutant, it is specifically compromised in Fe-S cluster biogenesis, as it lacks both the scaffold for assembling the Fe-S cluster and the transport machinery that inserts the Fe-S cluster into apo-proteins (9, 10). Interestingly, the *iscUA* mutant was resistant to Gm and sensitive to Amp in all tests used (Fig. 2, A and B, table S1, and fig. S5). We conclude that Fe-S clusters are required for the bactericidal effect of aminoglycosides but not for that of  $\beta$ -lactams.

If killing by aminoglycosides is not caused by ROS, why does eliminating the ISC system render *E. coli* resistant to these antibiotics? Fe-S clusters are essential for growth, and *E. coli* has a second assembly system, called SUF (10). To

<sup>1</sup>Laboratoire de Chimie Bactérienne, Aix-Marseille Université, CNRS, UMR 7283, Institut de Microbiologie de la Méditerranée, 31 Chemin Joseph Aiguier, 13009 Marseille France. <sup>2</sup>Genome Biology Unit, European Molecular Biology Laboratory, Meyerhofstrasse 1, 69117 Heidelberg, Germany.

\*Corresponding author. E-mail: barras@imm.cnrs.fr